

Orientalional Dichroism in the Electron-Impact Ionization of Laser-Oriented Atomic Sodium

A. Dorn,* A. Elliott, J. Lower, E. Weigold, and J. Berakdar†

*Atomic and Molecular Physics Laboratories, Research School of Physical Sciences and Engineering,
Australian National University, Canberra ACT 0200, Australia*

A. Engelns and H. Klar

Fakultät für Physik, Albert-Ludwigs-Universität, Hermann-Herder-Strasse 3, 79104 Freiburg, Germany

(Received 11 September 1997)

We report the first experimental observation of “orientational dichroism” in electron impact-induced ionization. ($e, 2e$) experiments have been performed on pure angular momentum states $3P_{3/2}$, $m_F = +3$ and $m_F = -3$ of the sodium atom, excited by right- and left-handed circularly polarized laser light. Our results show that the angular correlation of the final-state electron pair is strongly dependent on the m_L sublevel populated. Comparison with calculation demonstrates the dependence of the dichroism on details of the scattering dynamics. [S0031-9007(97)04999-5]

PACS numbers: 34.80.Dp

A detailed knowledge of the ionization process is essential to our understanding of, and progress in, such diverse fields as discharge and plasma physics, fusion physics, laser physics, and the physics and chemistry of the upper atmosphere. The most accurate information on this process is derived from kinematically complete ($e, 2e$) experiments, in which the energies and momenta of all reaction participants and products are determined [1]. We report here on an ($e, 2e$) experiment in which the projection quantum number for an excited atomic target in a pure nonzero angular momentum state is also resolved. Using laser pumping techniques, an atomic sodium target is laser excited to the $3^2P_{3/2}F = 3$, $m_F = +3$ or $m_F = -3$ hyperfine states. These states consist of maximal projections of the nuclear spin ($I = \pm 3/2$), the orbital angular momentum ($m_L = \pm 1$), and the electron spin ($S = \pm 1/2$) along the laser beam direction.

If neither the projection quantum numbers of the incident electron nor the target are resolved, the ($e, 2e$) differential cross section is simply a scalar invariant with respect to a joint rotation of the incoming and outgoing electron momenta \mathbf{p}_0 , \mathbf{p}_a , and \mathbf{p}_b , respectively. This basic symmetry is destroyed by an initial orientation and/or alignment of the target. The ($e, 2e$) cross section is then irreducibly described by a set of tensorial parameters whose number is determined by the symmetry of the initially prepared target state [2]. Generally, the cross section for the ionization of a target with total angular momentum J can be written as [2]

$$\frac{d^5\sigma}{d\Omega_a d\Omega_b dE_b} = \sum_{i=0}^{2J} \rho_{i0} \Lambda_0^{(i)}, \quad (1)$$

where $\Lambda_0^{(i)}$ are tensorial components along the quantization axis of the target describing the dynamics of the ionization process and ρ_{i0} are the state multipoles describing the M-state population of the target. The transformation properties of $\Lambda_0^{(i)}$ are determined by the rank i of the

associated tensor. The solid angles of the momenta \mathbf{p}_a , \mathbf{p}_b with respect to \mathbf{p}_0 are labeled by $d\Omega_a$, $d\Omega_b$, respectively.

In the present case of the Na $3P_{3/2}$ state, neglecting spin-orbit interactions and for unpolarized primary electrons it suffices to consider Eq. (1) with respect to the orbital angular momentum $L = 1$ for singlet and triplet scattering. Then the cross section is described only by three tensorial components $\Lambda_0^{(i)}$, which can be written in terms of the ionization cross sections for the individual magnetic substates σ_{L,m_L} :

$$\Lambda_0^{(0)} = \frac{1}{\sqrt{3}} (\sigma_{1,1} + \sigma_{1,0} + \sigma_{1,-1}), \quad (2)$$

$$\Lambda_0^{(1)} = \frac{1}{\sqrt{2}} (\sigma_{1,1} - \sigma_{1,-1}), \quad (3)$$

$$\Lambda_0^{(2)} = \frac{1}{\sqrt{6}} (\sigma_{1,1} - 2\sigma_{1,0} + \sigma_{1,-1}). \quad (4)$$

The scalar component $\Lambda_0^{(0)}$ yields the averaged triply differential cross section for statistically populated m_L states, while the deviation of this cross section from that for the ionization of the $m_L = 0$ state is indicated by the alignment component $\Lambda_0^{(2)}$. The quantity $\Lambda_0^{(1)}$ is a vector component and is a measure of the change in the cross section resulting from an inversion of the initial target orientation. An understanding of the geometrical and dynamical properties of $\Lambda_0^{(1)}$ yields direct insight into the transfer of initial state orientation to the two-electron continuum final state. In the present experiment we measure all of the parameters in Eqs. (2)–(4) as $\sigma_{1,0}$ is zero due to the experimental arrangement (Fig. 1), the $3P_{m_L=0}$ wave function having a node in the scattering plane.

Only a brief description of the experimental apparatus will be given here (shown schematically in Fig. 1) with attention focused on the new elements, namely, the sodium source and the laser pumping system incorporated into our previously described polarized electron spectrometer [3].

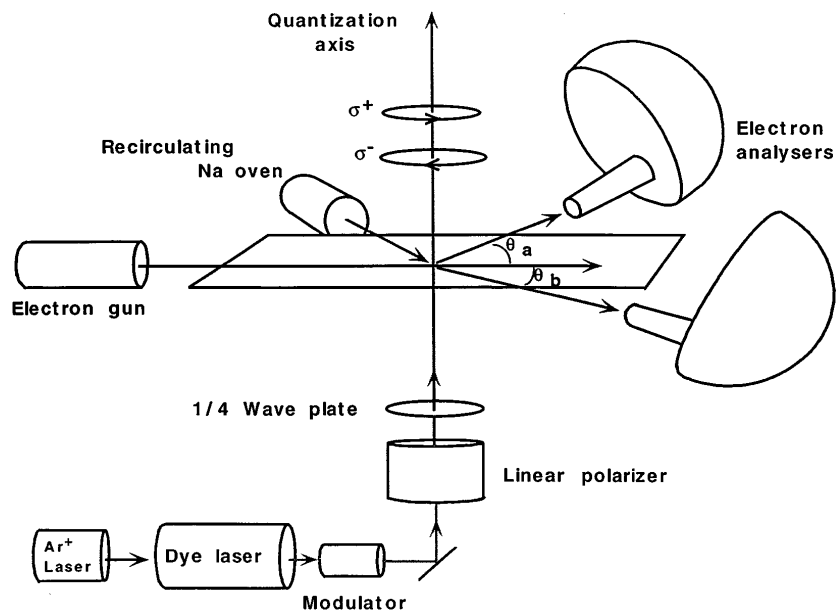


FIG. 1. Schematic representation of the apparatus.

In the apparatus, a beam of unpolarized electrons is produced by photoemission from a negative electron affinity GaAs crystal surface. The target beam of sodium atoms is produced by effusion of sodium gas through a 1 mm aperture positioned at the output stage of a recirculating oven. The oven [4] is similar in design to that of McClelland *et al.* [5] and is housed in a water cooled containment box upon which a liquid nitrogen cooled collimating aperture and sodium beam dump is mounted.

Intersecting at right angles the plane defined by the electron and sodium beams, and completely encompassing the region formed by their overlap, is a 589 nm laser beam used to excite the sodium atoms. The initially linearly polarized laser light is converted to circularly polarized radiation by transmission through a quarter wave plate, the rotation of which by 90° reverses the helicity of the radiation field. In order to reach a high fraction of laser excited atoms in the scattering volume, the laser excitation is performed by means of two laser frequencies produced by frequency modulation of a single mode dye-laser beam. One frequency is tuned to the transition $3S_{1/2}(F=2) \rightarrow 3P_{3/2}(F=3)$, the other is tuned to the transition $3S_{1/2}(F=1) \rightarrow 3P_{3/2}(F=2)$. In this way a relative fraction of about 40% $3P_{3/2}$ states is reached [6]. Despite the fact that the $3P_{3/2}(F=2)$ level is pumped, after a few excitation/decay cycles the atoms gather in the two level system $3S_{1/2}(F=2, m_F=\pm 2) \leftrightarrow 3P_{3/2}(F=3, m_F=\pm 3)$ only. This is confirmed numerically by solving the corresponding rate equations. The degree of orientation of the excited state in the scattering volume was between 96% and 100%. This was checked by comparing our superelastic scattering data with those of [5].

The analyzers [3] incorporate position sensitive detectors at their exit plane, enabling simultaneous measure-

ment over a 6 eV energy band with a resolution of around 0.2 eV. A total coincidence ($e, 2e$) resolution of around 0.9 eV was achieved, more than sufficient to accurately distinguish between ionizing events occurring from atoms in their ground and excited states, which are separated in binding energy by 2.14 eV. The cross sections σ_{L, m_L} with $L=1, m_L=\pm 1$ are given by

$$\sigma_{1, \pm 1} = C |\langle \Psi(\mathbf{r}_a, \mathbf{r}_b) | V | \varphi_{p_0}(\mathbf{r}_a) \Phi_{1, \pm 1}(\mathbf{r}_b) \rangle|^2, \quad (5)$$

where $C = (2\pi)^4 p_a p_b / p_o$, and $\mathbf{r}_a, \mathbf{r}_b$ are, respectively, the positions of the projectile and the valence electron with respect to the nucleus. The initial state is described by a direct product of a plane wave $\varphi_{p_0}(\mathbf{r}_a)$ describing the incoming projectile and an undistorted bound state $\Phi_{L=1, m_L=\pm 1}(\mathbf{r}_b)$ for the laser-pumped Na. The perturbation operator V is then the Coulombic interaction of the projectile with the active electron and the core.

We have performed three calculations to evaluate the cross sections (5). In all cases, the motion of the valence electron is calculated assuming single particle motion around a frozen core. In the first calculation, the model Klapisch potential is employed for this purpose [7,8]:

$$V_{\text{Na}} = \frac{-1}{r_b} - \frac{Z-1}{r_b} \exp(-\alpha_1 r_b) - \alpha_3 \exp(-\alpha_2 r_b), \quad (6)$$

with $Z=11$, $\alpha_1=7.902$, $\alpha_2=2.688$, and $\alpha_3=23.51$. The final two-electron continuum state in the field of Na^+ [$\Psi(\mathbf{r}_a, \mathbf{r}_b)$ in Eq. (5)] is approximated by a product of three two-body Coulomb waves with dynamical coupling between the individual two-body subsystems being included (hereafter DS3C) [9]:

$$\begin{aligned} \Psi(\mathbf{r}_a, \mathbf{r}_b) \approx & N e^{i\mathbf{p}_a \cdot \mathbf{r}_a} e^{i\mathbf{p}_b \cdot \mathbf{r}_b} {}_1F_1[i\beta_a, 1, -i(p_a r_a + \mathbf{p}_a \cdot \mathbf{r}_a)] \\ & \times {}_1F_1[i\beta_b, 1, -i(p_b r_b + \mathbf{p}_b \cdot \mathbf{r}_b)] \\ & \times {}_1F_1[i\beta_{ab}, 1, -i(p_{ab} r_{ab} + \mathbf{p}_{ab} \cdot \mathbf{r}_{ab})], \end{aligned} \quad (7)$$

where $\mathbf{r}_{ab} = \mathbf{r}_a - \mathbf{r}_b$ and \mathbf{p}_{ab} its conjugate momentum. ${}_1F_1[a, b, c]$ is the confluent hypergeometric function and N is a normalization factor. The explicit form of the dynamical Sommerfeld parameters β_j , $j = a, b, ab$ has been given elsewhere [10].

The second calculation differs in two respects from the former. First, the Danielle potential is used to calculate the motion of the valence electron [11–13]:

$$\begin{aligned} V_{\text{eff}}(r) = & \frac{-1}{r} \left\{ \left[2 + \frac{4}{3} \gamma_1 r + \frac{1}{3} (\gamma_1 r)^2 \right] \exp(-\gamma_1 r) \right. \\ & \left. + \left[8 + 6\gamma_2 r + 2(\gamma_1 r)^2 + \frac{1}{3} (\gamma_2 r)^3 \right] \right. \\ & \left. \times \exp(-\gamma_1 r) \right\}, \end{aligned} \quad (8)$$

with $\gamma_1 = 2.026$ and $\gamma_2 = 5.254$. Second, the final two-electron continuum state is represented by the correlated Brauner-Briggs-Klar (BBK) wave function [13,14]. This is identical in form to (7) except that in this case the standard Sommerfeld parameters [15] are used in place of the dynamical Sommerfeld parameters.

The final calculation is the first Born approximation (FBA) which was obtained from Eqs. (6) and (7) in the limit $\beta_a \equiv 0 \equiv \beta_{ab}$. Within the FBA and for hydrogenic targets [16] the dichroism (3) possesses the structure $\Lambda_0^{(1)} \propto \hat{\mathbf{e}}_z \cdot (\mathbf{q} \times \mathbf{p}_b)$ with $\hat{\mathbf{e}}_z$ being the quantization axis of the target and $\mathbf{q} = \mathbf{p}_0 - \mathbf{p}_a$ is the momentum transfer, i.e., for a given \mathbf{q} , the angular dependence of $\Lambda_0^{(1)}(\hat{\mathbf{p}}_b)$ shows a reflection antisymmetry with respect to $\hat{\mathbf{q}}$, and hence $\Lambda_0^{(1)}(\hat{\mathbf{p}}_b)$ vanishes at $\hat{\mathbf{p}}_b \parallel \hat{\mathbf{q}}$ (in the present Letter the direction $\hat{\mathbf{e}}_z$ is perpendicular to the scattering plane spanned by $\hat{\mathbf{p}}_b$, $\hat{\mathbf{p}}_a$, and $\hat{\mathbf{p}}_0$). To verify these predictions two separate ($e, 2e$) experiments were performed under coplanar asymmetric scattering geometry and their results compared to our calculations. The experiments consisted of measuring the ($e, 2e$) ionization cross section for a fixed scattering angle θ_a of the fast emitted electron as a function of the scattering angle θ_b for the slow electron and for both positive ($m_L = +1$) and negative ($m_L = -1$) orbital orientations of the excited state.

In the first run, the incident beam energy was 150 eV, the detection angle for the fast outgoing electrons was 20° , and the slow electrons were measured over an energy band of 20 ± 3 eV. Under these conditions of moderately high values of incident energy the FBA might be reasonably valid. The existence and the transformation properties of $\Lambda_0^{(1)}$, i.e., the reflection symmetry between $\sigma_{1,\pm 1}$ about $\hat{\mathbf{q}}$, are evident from Fig. 2. The FBA adequately describes the behavior of $\Lambda_0^{(1)}$; however the calculation does show a

hardly perceptible break in the reflection antisymmetry at $\hat{\mathbf{q}}$. This is due to the fact that the final state of the valence electron is chosen as a pure hydrogenic continuum state whereas (6) is not pure hydrogenic, i.e., initial and final states of the ejected electron are not orthogonal which leads to a finite scattering from the core and hence the slight break in the symmetry, as observed in Fig. 2. As expected at 150 eV the DS3C calculation is quite close in shape to the FBA, although the DS3C cross sections are moved to larger angles.

As in the isotropic target case [14], the FBA predicts larger cross sections than higher order theories. The data for $\sigma_{1,-1}$ have been normalized to the corresponding DS3C results. It should be stressed, however, that the normalized dichroism $\Lambda_0^{(1)}/\Lambda_0^{(0)}$ is uniquely determined by the experiment. The inset in Fig. 2 shows the binary peak in the cross section for the ionization from $\text{Na}(3^2S_{1/2})$ which is symmetric with respect to $\hat{\mathbf{q}}$, and again agrees quite well in shape with the FBA.

For our second measurement, the incident beam energy was lowered to 60 eV for the same fast electron scattering angle θ_a and slow electron energy band of 20 ± 3 eV (Fig. 3). The FBA is not capable of describing the complicated ($e, 2e$) scattering dynamics at intermediate and low energies and thus in this case a much more complicated structure for $\Lambda_0^{(1)}$ is anticipated. Indeed, from Fig. 3 it is immediately clear that the FBA (which is not plotted here) cannot account for the behavior of

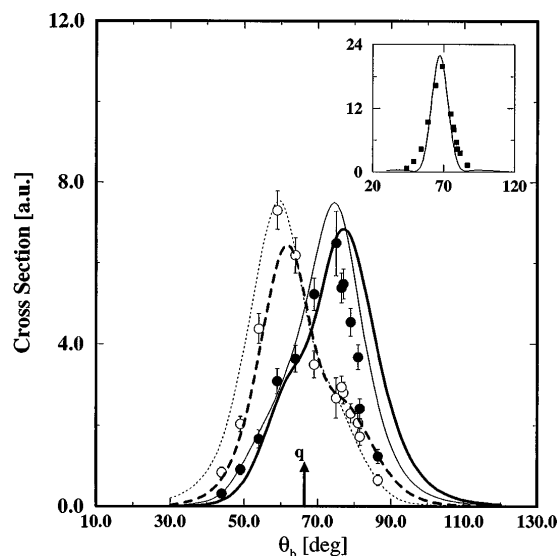


FIG. 2. The 150 eV ($e, 2e$) cross section on $\text{Na } 3^2P_{3/2}$, $m_F = -3$ (filled circles) and $m_F = +3$ (open circles) for $\theta_a = 20^\circ$, $\phi_a - \phi_b = \pi$, and $\bar{E}_b = 20$ eV. The corresponding FBA (scaled down by a factor of 2) and DS3C cross sections are indicated, respectively, by thin solid and dotted lines and thick solid and dashed lines. The measurements are normalized to the $m = -1$ DS3C cross section peak. The momentum transfer direction is given by \mathbf{q} . The inset shows the ground state $\text{Na } 3^2S_{1/2}$ transition normalized to the FBA cross section.

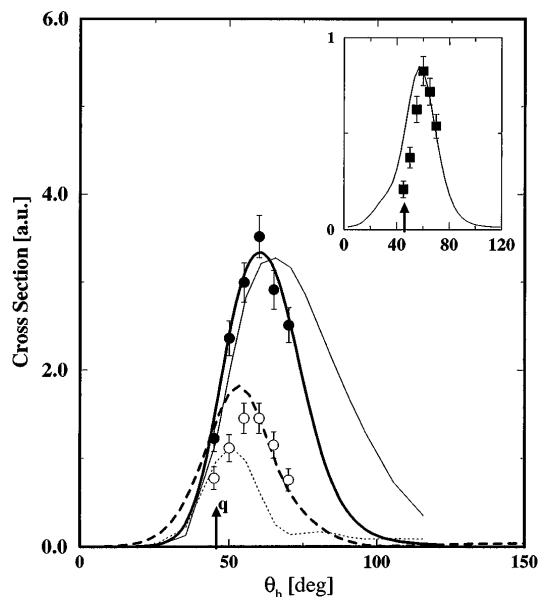


FIG. 3. As in Fig. 2 except for incident energy of 60 eV. In addition to the DS3C calculations, the calculations using the BBK final state (multiplied by 1.5) are shown as thin dashed and dot-dashed curves for, respectively, the $m_L = -1$ and $m_L = +1$ transitions. Inset shows the ground state cross section normalized to the DS3C calculation (solid line).

$\Lambda_0^{(1)}$ as there is no reflection symmetry between the $m_L = \pm 1$ cross sections about the momentum transfer direction. The experimental data have been normalized to the DS3C calculation of $\sigma_{1,-1}$ at 60° . The DS3C calculations describe the experimental data quite well in shape, the angular positions of the cross section maxima, and the relative magnitudes. Also shown for comparison are the results of the BBK calculation. The difference between the two calculations shows their sensitivity to the treatment of the three-body final state. The shift of the measured cross section from the FBA predictions can be largely traced to final-state electronic correlations that are included in both the DS3C and BBK models. The use of the dynamical Sommerfeld parameters leads to cross sections in much better agreement with the data. The inset in Fig. 3 shows that the final-state correlations are also important for ground state ionization.

In summary the electron impact ionization of an oriented target leads to strong dichroism effects in the final state. The dependence of the cross section on the orienta-

tion of the initial state is dynamically related to the phase of the final-state wave function, which is a very sensitive quantity. At low energies final-state correlations are extremely important, significantly reducing the $m_L = +1$ cross section relative to the $m_L = -1$ cross section.

A.D. gratefully acknowledges support from the Deutsche Forschungsgemeinschaft and the Research School of Physical Sciences and Engineering at the Australian National University. J. B. acknowledges financial support by the Alexander von Humboldt Foundation.

*Present address: Fakultät für Physik, Albert-Ludwigs-Universität, Hermann-Herder-Strasse 3, 79104 Freiburg, Germany.

†Present address: Max-Planck Institute for Microstructure Physics, Weinberg 2, 06120 Halle, Germany.

- [1] I. E. McCarthy and E. Weigold, *Rep. Prog. Phys.* **54**, 789 (1991).
- [2] J. Berakdar, A. Engelns, and H. Klar, *J. Phys. B* **29**, 1109 (1996).
- [3] B. Granitza, X. Guo, J. M. Hurn, J. Lower, S. Mazevet, I. E. McCarthy, Y. Shen, and E. Weigold, *Aust. J. Phys.* **49**, 383 (1996).
- [4] Y. Shen, Ph.D. thesis, Australian National University, 1995 (unpublished).
- [5] J. J. McClelland, M. H. Kelly, and R. J. Celotta, *Phys. Rev. A* **40**, 2321 (1989).
- [6] E. E. B. Campbell, H. Hülser, R. Witte, and I. V. Hertel, *J. Phys. D* **16**, 21 (1990).
- [7] M. Klapisch, Ph.D. thesis, University of Paris-Sud Orsay, 1969.
- [8] C. Courbin, M. Machholm, and E. Lewartowski, *Z. Phys. D* **30**, 205 (1994).
- [9] J. Berakdar, *Phys. Rev. A* **53**, 2314 (1996).
- [10] J. Berakdar, J. Röder, J. S. Briggs, and H. Ehrhardt, *J. Phys. B* **29**, 1767 (1996).
- [11] R. Danielle, *J. Chem. Phys.* **70**, 3462 (1979).
- [12] R. Danielle, *J. Chem. Phys.* **72**, 1276 (1980).
- [13] A. Engelns, Ph.D. thesis, University Freiburg (unpublished).
- [14] M. Brauner, J. Briggs, and H. Klar, *J. Phys. B* **22**, 2265 (1989).
- [15] J. Berakdar and H. Klar, *J. Phys. B* **26**, 4219 (1993).
- [16] M. Fehr, J. Berakdar, and H. Klar, *J. Phys. B* **27**, L401 (1995).